Nano Res. 2012, 5(1): 20–26
DOI 10.1007/s12274-011-0180-3
Research Article

ISSN 1998-0124
CN 11-5974/O4

Sulfur-Doped Zinc Oxide (ZnO) Nanostars: Synthesis and Simulation of Growth Mechanism

Jinhyun Cho[1], Qiubao Lin[2,3], Sungwoo Yang[2], Jay G. Simmons Jr.[2], Yingwen Cheng[2], Erica Lin[2], Jianqiu Yang[2], John V. Foreman[4], Henry O. Everitt[4,5], Weitao Yang[2], Jungsang Kim[1], and Jie Liu[2] (✉)

[1] Department of Electrical and Computer Engineering, Fitzpatrick Institute for Photonics, Duke University, Durham, North Carolina 27708, USA
[2] Department of Chemistry, French Family Science Center, Duke University, Durham, North Carolina 27708, USA
[3] School of Science, Jimei University, Xiamen 361021, China
[4] U.S. Army Aviation and Missile Research, Development, and Engineering Center, Weapons Sciences Directorate, Redstone Arsenal, AL 35898, USA
[5] Department of Physics, Duke University, Durham, NC 27708, USA

Received: 23 June 2011 / Revised: 17 October 2011 / Accepted: 19 October 2011

ABSTRACT

We present a bottom-up synthesis, spectroscopic characterization, and *ab initio* simulations of star-shaped hexagonal zinc oxide (ZnO) nanowires. The ZnO nanostructures were synthesized by a low-temperature hydrothermal growth method. The cross-section of the ZnO nanowires transformed from a hexagon to a hexagram when sulfur dopants from thiourea [$SC(NH_2)_2$] were added into the growth solution, but no transformation occurred when urea ($OC(NH_2)_2$) was added. Comparison of the X-ray photoemission and photoluminescence spectra of undoped and sulfur-doped ZnO confirmed that sulfur is responsible for the novel morphology. Large-scale theoretical calculations were conducted to understand the role of sulfur doping in the growth process. The *ab initio* simulations demonstrated that the addition of sulfur causes a local change in charge distribution that is stronger at the vertices than at the edges, leading to the observed transformation from hexagon to hexagram nanostructures.

KEYWORDS

ZnO nanostar, hexagram, thiourea, sulfur doping, growth mechanism, *ab initio* simulation

1. Introduction

Zinc oxide (ZnO) is a wide bandgap (3.37 eV), Ⅱ–Ⅵ semiconductor of great interest for optoelectronic applications [1–3]. Its advantages over other wide band gap materials include eco-friendliness, resistance to oxidation, low cost, and a large exciton binding energy (60 meV) [4]. In terms of optical properties, ZnO has two well-documented emission bands of varying strengths: the band edge ultraviolet (UV) emission and a broad, defect-mediated green emission [1, 3]. The microscopic origin of the emission in the green spectral band has been attributed to intrinsic defects, such as oxygen vacancies and zinc interstitials, that serve as trap centers for the electron–hole recombination, or to external dopants such as sulfur, and is broadened

Address correspondence to j.liu@duke.edu

by the emission of multiple longitudinal-optical (LO) phonons [1, 2, 4, 5]. Variously shaped ZnO nanowires and nanoparticles are routinely synthesized, and their electrical and optical properties have been exploited for many exciting applications including nanolasers, phosphors, light emitting diodes, biosensors, solar cells, and electrical generators [1, 6–11]. ZnO nanostructures offer new and enhanced properties that differ from the bulk powder due to their high surface-to-volume ratio [1, 12] and can be prepared using chemical vapor deposition (CVD) or solution-based methods. For large-scale applications, the solution-based method is more attractive than CVD since no expensive equipment is required [13, 14].

When ZnO nanostructures are synthesized, the polar nature of the wurtzitic ZnO lattice causes preferential growth along certain crystal facets [15], leading to a wide range of nanostructure morphologies depending on the details of the growth conditions [16–21]. Although various ZnO nanostructures have been discovered [16–21], there have been no systematic studies combining experimental measurements with *ab initio* theoretical calculations to explore why complex ZnO nanostructures evolve the way they do during growth. Understanding the detailed growth dynamics may allow a more controlled manipulation of nanostructure shape, guiding the fabrication of unique nanostructures with tailored or unusual properties [22].

In this article, we report the synthesis of hexagram-shaped ZnO nanostructures ("nanostars") by sulfur-doping hexagonal ZnO nanowires with thiourea ($SC(NH_2)_2$) in a low-temperature solution-based process. Scanning electron microscopy (SEM) reveals that the cross-sectional shape of the nanostructure strongly depends on sulfur doping levels. Density functional theory calculations suggest that the evolution from hexagonal nanowires to nanostars during growth occurs because sulfur atoms preferentially attach to the hexagonal vertices. The resulting change in the local chemical environment is the likely origin of the observed hexagram structure. The presence of sulfur in the nanostars was confirmed using X-ray photoelectron spectroscopy (XPS) and photoluminescence (PL) spectroscopy. Control experiments replacing thiourea with its sulfur-free analog urea ($OC(NH_2)_2$) confirmed the role of sulfur in the growth of nanostars.

2. Experimental

The ZnO nanowires were synthesized in solution according to the procedures of Greene and Pacholski [13, 23]. In this approach, solutions of 0.01 mol/L zinc acetate dihydrate [$(CH_3CO_2)_2Zn{\cdot}2H_2O$ (Fluka, assay ≫ 99.5%)] and 0.03 mol/L sodium hydroxide [NaOH (Fisher Chemical, assay = 98.6%)] in methanol were first prepared. Then, 26.32 mL of 0.01 mol/L $(CH_3CO_2)_2Zn{\cdot}2H_2O$ solution and 13.68 mL of 0.03 mol/L NaOH solution were combined and stirred for 2 h at 60 °C. The resulting solution was used to create ZnO seed crystals by drop-coating onto a silicon substrate, rinsing with methanol, and blow-drying with air. This drop-coating process was repeated several times. The ZnO seed crystals were then formed by annealing the substrate at 350 °C for 20 min.

Hydrothermal growth of the ZnO nanowires was achieved by placing the substrate in an aqueous solution containing 0.025 mol/L zinc nitrate [$Zn(NO_3)_2{\cdot}xH_2O$ (Alfa Aesar, assay = 99%)] and 0.025 mol/L hexamine (hexamethylenetetramine) [$(CH_2)_6N_4$ (Alfa Aesar, assay = 98%)] and heating this solution to 90–95 °C for 2 h. The ZnO nanostars studied in this report were obtained by adding various concentrations of a thiourea [$SC(NH_2)_2$ (Alfa Aesar, assay = 99%)] doping solution to the hydrothermal growth process. The thiourea concentration was varied (0.025 mol/L, 0.05 mol/L, 0.1 mol/L, 0.2 mol/L, and 0.5 mol/L), and a control experiment was also performed with 0.1 mol/L urea [$OC(NH_2)_2$ (Acros Organics, assay = 99%)]. In each experiment 10 mL of each reactant solution was used. For each of the thiourea-doped growth solutions the total volume was 30 mL. All products were characterized by SEM (FEI XL 30), PL, and XPS (Kratos Analytical Axis Ultra). PL measurements were performed at room temperature using the 325 nm line of a HeCd laser and a HORIBA Jobin Yvon LabRAM ARAMIS grating spectrometer.

3. Results and discussion

A systematic evolution from hexagon- to hexagram-shaped nanostructures was observed as the concentration of thiourea was increased in the growth solution. Figure 1 shows SEM images of the resulting

nanowires as the concentration of thiourea was increased. Without the addition of thiourea, undoped ZnO nanowires showed a typical hexagonal cross-section in their top surfaces (Fig. 1(a)). Addition of a low concentration [0.025 mol/L] of thiourea led to the growth of material on the outside edges of the nanowires and resulted in a circular cross-section (Fig. 1(b)). As the concentration of thiourea was increased to 0.05 mol/L (ratio of zinc nitrate, hexamine, and thiourea = 1:1:2), the cylindrical cross-section evolved into a flower-like cross-section (Fig. 1(c)). Upon increasing the concentration of thiourea further to 0.1 mol/L and 0.2 mol/L (ratios of zinc nitrate, hexamine, and thiourea = 1:1:4 and 1:1:8, respectively), ZnO nanostars with hexagram cross-sections were generated (Figs. 1(d) and 1(e)). It is noteworthy that the nanowire diameters depend on the growth parameters such as seed coating conditions, initial seed size, growth temperature, and kinetics. Increasing the thiourea concentration beyond 0.2 mol/L did not lead to the creation of ZnO nanostars, but rather to circular-shaped aggregates (see Fig. S-1 in the Electronic Supplementary Material (ESM)). This suggests that there is an optimum molar ratio of original nutrient component to thiourea for the growth of the hexagram structures.

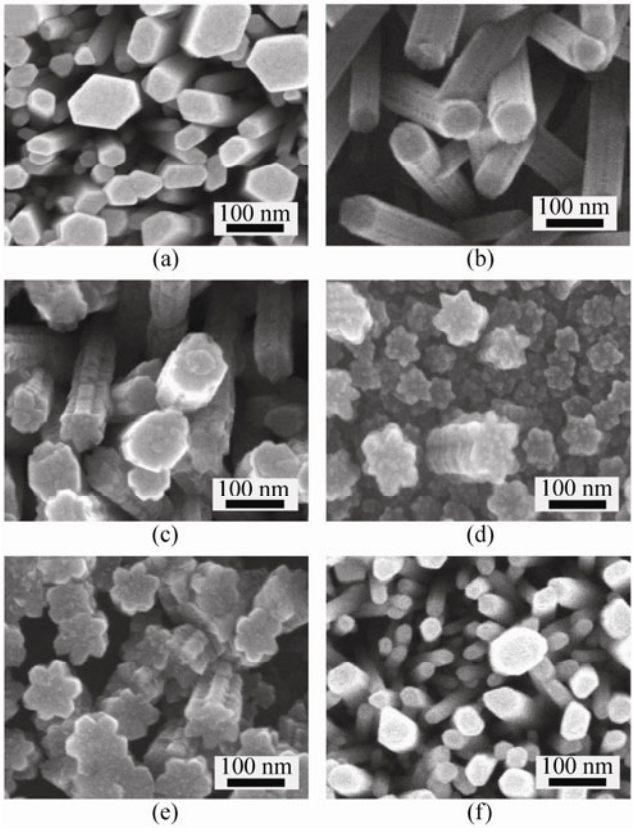

Figure 1 SEM images of ZnO nanostructures synthesized from the mixed aqueous solutions of 0.025 mol/L zinc nitrate and 0.025 mol/L hexamine with (a) no thiourea, (b) 0.025 mol/L thiourea, (c) 0.05 mol/L thiourea, (d) 0.1 mol/L thiourea, (e) 0.2 mol/L thiourea, and (f) 0.1 mol/L urea as a control sample

To verify the role of sulfur in the formation of the hexogram nanostars, a control experiment was performed by replacing thiourea with urea ($OC(NH_2)_2$). The molecular structure of urea is identical to thiourea, except that the sulfur atom is replaced by an oxygen atom. Addition of 0.1 mol/L urea solution did not lead to any deviation from the hexagonal cross-section of standard ZnO (Fig. 1(f)), confirming the importance of sulfur in the structural change.

XPS was also performed on these samples to detect the presence of sulfur at the surface of the nanostructures directly. Figure 2(a) shows the averaged atomic concentrations of sulfur obtained by XPS for the samples in Figs. 1(b)–1(e). As thiourea concentration was increased, the average sulfur concentration increased accordingly. In addition, Fig. 2(b) shows that the averaged core-level spectra of the sulfur 2p peak gradually increases with increasing sulfur concentration as the morphology varies as shown in Figs. 1(a)–1(e).

The correlation between the cross-sectional shape of the nanostructures and presence of sulfur suggests that sulfur is responsible for creating the sharp points of the hexagram structure. To confirm this, we performed an additional experiment to correlate the sharp points of the hexagram with presence of sulfur. First, standard hexagonal ZnO nanowires were grown in the original growth solution of 0.025 mol/L zinc nitrate and 0.025 mol/L hexamine. Then, these hexagonal nanowires were either re-grown in an identical growth solution (Fig. 3(a)) or in a mixed growth solution with 0.1 mol/L thiourea (Fig. 3(b)). The re-grown sulfur-free ZnO nanowires (Fig. 3(a)) show hexagonal cross-sections identical to the original nanowires in Fig. 1(a). However, the re-growth of hexagonal nanowires with thiourea produced the hexagram cross-sectional shape as shown in Fig. 3(b), suggesting that the sharp points have been "added" to the hexagonal cross-section.

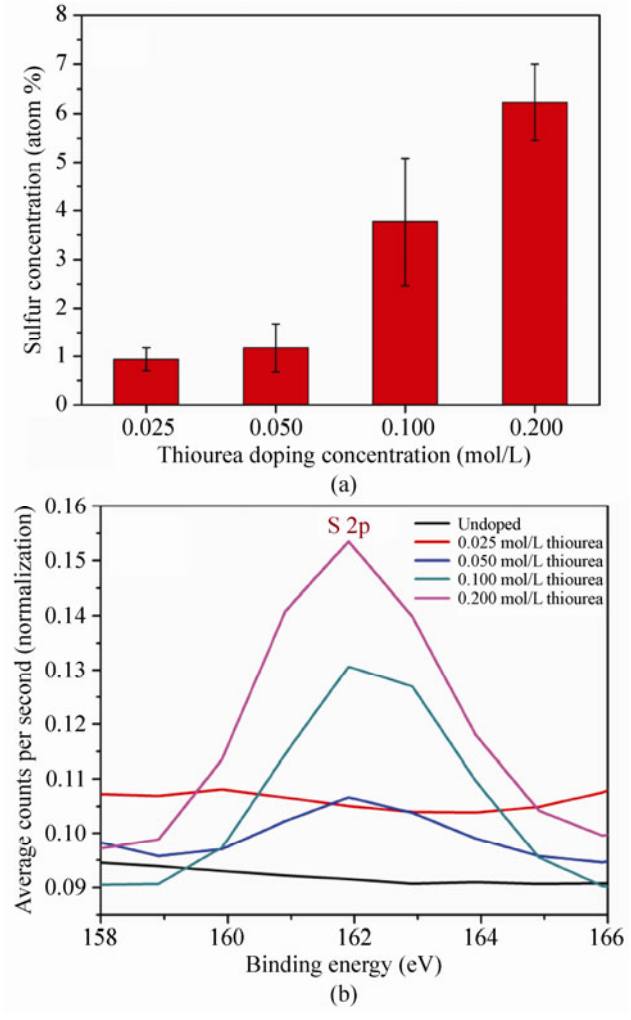

Figure 2 (a) Averaged sulfur concentrations obtained by XPS of various thiourea-doped ZnO nanostructures; (b) averaged core-level XPS corresponding to the sulfur 2p peak for ZnO nanostructures with various concentrations of thiourea. Black, red, blue, green, and pink lines indicate undoped, 0.025 mol/L, 0.050 mol/L, 0.1 mol/L, and 0.2 mol/L thiourea doped samples, respectively

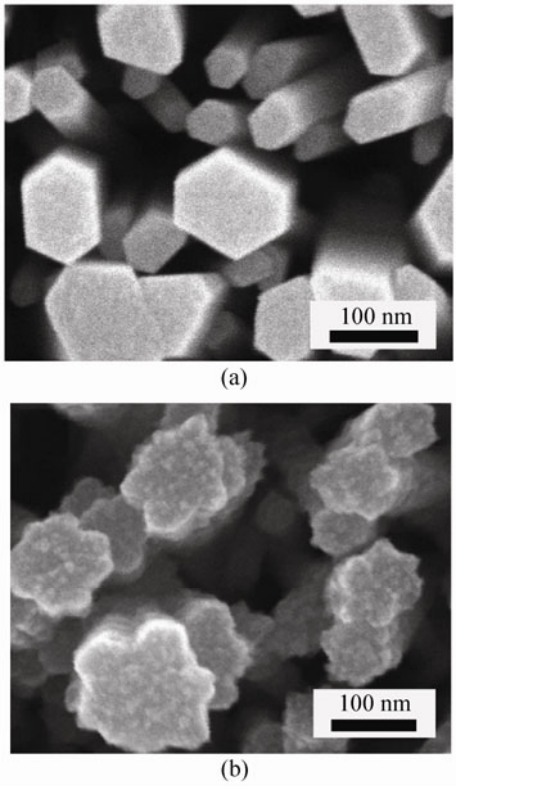

Figure 3 (a) SEM images of re-grown nanowires in the absence of thiourea dopant and (b) after re-growth in a mixture of 0.025 mol/L zinc nitrate, 0.025 mol/L hexamine, and 0.1 mol/L thiourea

In order to understand the role of sulfur in the formation of the nanostars, the energy configurations corresponding to two distinct types of nanowire structure were calculated. First, the ZnO nanowires were modeled as hexagonal wurtzite structures (space group *C*6*mc*) with lattice parameters $a = 0.3296$ nm and $c = 0.52065$ nm. Then, in one scenario, sulfur atoms replace the oxygen atoms at the corners of the nanowire surface (Fig. 4(a)), while in the other scenario, sulfur atoms replace the oxygen atoms at the edges of the nanowire surface (Fig. 4(b)). The binding energy for each scenario was calculated using the Vienna *ab initio* simulation package (VASP) [24, 25], which is based on the density functional theory in the plane-wave basis and the projector augmented wave (PAW) representation. The exchange and correlation energies were described by the generalized gradient approximation (GGA) of Perdew et al. [26]. Brillouin-zone integrations were approximated by using the special 1 × 1 × 30 grid *k*-point sampling of the Monkhorst–Pack scheme [27] for the nanowire (the *z*-direction is chosen as the nanowire axis), in conjunction with the Gaussian-smearing method with $\sigma = 0.01$ eV. The cutoff for the plane-wave kinetic energy in this calculation was chosen to be 400 eV. The convergence of the total energy with respect to *k*-point sampling (Table 1) and the plane-wave energy cut-off were both examined.

The calculations indicated that the sulfur-replacement binding energy is 0.04 eV higher per atom with corner replacement than with edge replacement. In other words, the corner replacement of oxygen by sulfur is significantly more favorable, suggesting a preferred pathway for the growth of sulfur-doped nanostructures. Sulfur atoms provided by thermally decomposed

Table 1 Calculated total energy of the supercell as a function of the number of *k*-points used

Number of *k*-points	1	30	40
E_1 (eV)	–453.884765	–445.646002	–445.648226
E_2 (eV)	–453.256291	–445.405713	–445.407931
$E_2 - E_1$ (eV)	0.628474	0.240289	0.240295

E_1: The total energy of the supercell with corner replacement by six S atoms per plane.
E_2: The total energy of the supercell with edge replacement by six S atoms per plane.

thiourea prefer to bind at the stable corner sites, thereby hindering growth from the corners. Wedge-shaped growth of the S-doped material from the edges leads to the observed hexagram-shaped structures. This wedge-shaped growth occurs because of differences in the Zn–S bonds between the corner and edge replacement configurations. In edge replacement, one of the three zinc ions bonded with a sulfur ion has a dangling bond, whereas in corner replacement, two of the three zinc ions have a dangling bond. These different bond configurations are caused by differences in the charge density distribution that ultimately affect the structural stability. This can be seen in Fig. 4(c), which shows a plot of the calculated charge density difference $\Delta\rho = \rho_2 - \rho_1$ in the plane of the Zn atoms in units of e/Å^3, where ρ_2 is the charge density after edge replacement, and ρ_1 is the charge density after corner replacement in plane $\{01\bar{1}\frac{8}{15}\}$ but shifted to the same replacement position to enable direct subtraction. The white areas represent regions in the plane of Zn atoms with (unplotted) large charge density variations (> 0.015 e/Å^3) of little interest because they are far removed from the region of the S atom. Small but important charge density differences are revealed in Fig. 4(c) near the region of the sulfur atom. Specifically, the blue region in the plane beneath the position of the sulfur nucleus, where $\Delta\rho \approx -0.01$ e/Å^3, shows that electrons are concentrated more tightly near the sulfur atom in the corner replacement geometry. This confirms the stronger bond strength that makes corner replacement more stable.

The optical properties of the nanostars were studied by PL spectroscopy using a 325 nm HeCd laser as a pump source at room temperature. Figure 5 shows

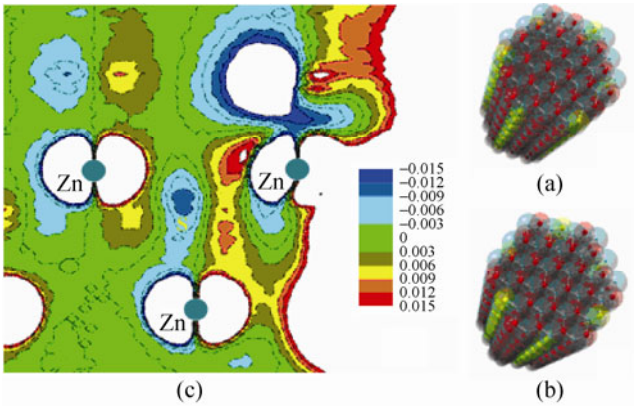

Figure 4 (a) O (red) is replaced by S (yellow) at the corners of the nanowire surface; (b) O (red) is replaced by S (yellow) at the edges of the nanowire surface; (c) a spatial contour plot of the charge density difference (units of e/Å^3) between edge and corner replacement of S calculated in the $\{01\bar{1}\frac{8}{15}\}$ plane of Zn atoms in the surface. The yellow letter "S" indicates the position of the S nucleus above this plane

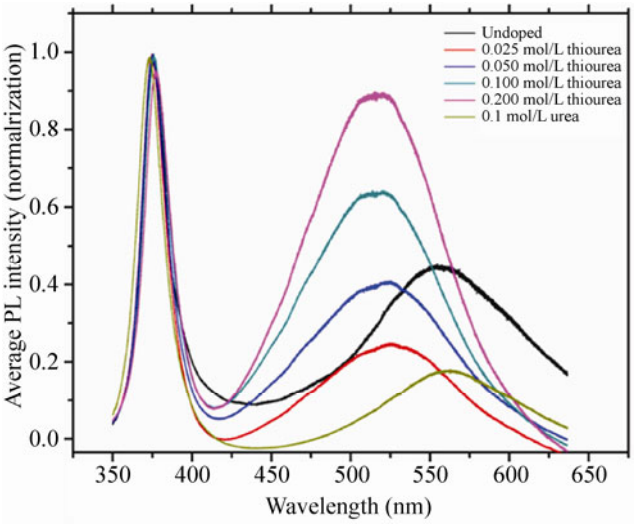

Figure 5 Superimposed PL spectra of samples of ZnO nanostars fabricated from a mixed aqueous solution of 0.025 mol/L zinc nitrate, 0.025 mol/L hexamine, and various concentrations of thiourea, compared with undoped and 0.1 mol/L urea reference samples. Back, yellow, red, blue, green, and pink lines indicate undoped, 0.1 mol/L urea doped, 0.025 mol/L, 0.050 mol/L, 0.1 mol/L, and 0.2 mol/L thiourea doped samples, respectively

the normalized PL spectra of the ZnO nanowires doped with various thiourea concentrations. Undoped nanowires feature strong UV emission at the band edge (~375 nm) and weak visible emission centered near 557 nm. As the concentration of thiourea was increased, the visible emission was enhanced relative

to the UV emission, and the emission peak was blue-shifted to near 517 nm as expected for sulfur-doped ZnO [28]. No significant enhancement or blue-shift of the visible emission was observed in urea-doped samples.

4. Conclusions

We have developed a simple hydrothermal growth process for preparing sulfur-doped ZnO nanowires. As the doping level of sulfur was increased, the hexagonal nanowires developed into nanostars with a hexagram cross-section. The role of sulfur in the transformation of the cross-sectional morphology has been verified by various experiments and calculations. Sulfur-doped nanostar structures feature enhanced, slightly blue-shifted visible light emission, which might be of interest in visible light emitting device applications.

Acknowledgements

This work was supported by grants from Duke University, National Science Foundation (NSF) (Nos. ECCS-0925587 and CHE-09-11119), and the Science Foundation of Jimei University, China (No. ZQ2010006). The authors thank Professor Jeffrey Glass of Duke University for helpful discussions. The project also benefitted from access to the Duke Shared Materials Instrument Facility.

Electronic Supplementary Material: Supplementary material is available in the online version of this article at http://dx.doi.org/10.1007/s12274-011-0180-3.

References

[1] Foreman, J. V.; Li, J.; Peng, H.; Choi, S.; Everitt, H. O.; Liu, J. Time-resolved investigation of bright visible wavelength luminescence from sulfur-doped ZnO nanowires and micropowders. *Nano Lett.* **2006**, *6*, 1126–1130.

[2] Djurišić, A. B.; Leung, Y. H. Optical properties of ZnO nanostructures. *Small* **2006**, *2*, 944–961.

[3] Foreman, J. V.; Everitt, H. O.; Yang, J.; Liu, J. Influence of temperature and photoexcitation density on the quantum efficiency of defect emission in ZnO powders. *Appl. Phys. Lett.* **2007**, *91*, 011902.

[4] Özgür, Ü.; Alivov, Y. I.; Liu, C.; Teke, A.; Reshchikov, M. A.; Doğan, S.; Avrutin, V.; Cho, S. J.; Morkoç, H. A comprehensive review of ZnO materials and devices. *J. Appl. Phys.* **2005**, *98*, 041301.

[5] Reynolds, D. C.; Look, D. C.; Jogai, B. Fine structure on the green band in ZnO. *J. Appl. Phys.* **2001**, *89*, 6189–6191.

[6] Zhang, X. M.; Lu, M. Y.; Zhang, Y.; Chen, L. J.; Wang, Z. L. Fabrication of a high-brightness blue-light-emitting diode using a ZnO-nanowire array grown on *p*-GaN thin film. *Adv. Mater.* **2009**, *21*, 2767–2770.

[7] Yeh, P. H.; Li, Z.; Wang, Z. L. Schottky-gated probe-free ZnO nanowire biosensor. *Adv. Mater.* **2009**, *21*, 4975–4978.

[8] Weintraub, B.; Wei, Y.; Wang, Z. L. Optical fiber/nanowire hybrid structures for efficient three-dimensional dye-sensitized solar cells. *Angew. Chem. Int. Edit.* **2009**, *48*, 8981–8985.

[9] Wang, Z. L.; Song, J. Piezoelectric nanogenerators based on zinc oxide nanowire arrays. *Science* **2006**, *312*, 242–246.

[10] Wang, X.; Song, J.; Liu, J.; Wang, Z. L. Direct-current nanogenerator driven by ultrasonic waves. *Science* **2007**, *316*, 102–105.

[11] Xu, S.; Qin, Y.; Xu, C.; Wei, Y.; Yang, R.; Wang, Z. L. Self-powered nanowire devices. *Nat. Nanotechnol.* **2010**, *5*, 366–373.

[12] Shalish, I.; Temkin, H.; Narayanamurti, V. Size-dependent surface luminescence in ZnO nanowires. *Phys. Rev. B* **2004**, *69*, 245401.

[13] Greene, L. E.; Law, M.; Goldberger, J.; Kim, F.; Johnson, J. C.; Zhang, Y.; Saykally, R. J.; Yang, P. Low-temperature wafer-scale production of ZnO nanowire arrays. *Angew. Chem. Int. Edit.* **2003**, *42*, 3031–3034.

[14] Greene, L. E.; Law, M.; Tan, D. H.; Montano, M.; Goldberger, J.; Somorjai, G.; Yang, P. General route to vertical ZnO nanowire arrays using textured ZnO seeds. *Nano Lett.* **2005**, *5*, 1231–1236.

[15] Wang, Z. L. ZnO nanowire and nanobelt platform for nanotechnology. *Mat. Sci. Eng. R* **2009**, *64*, 33–71.

[16] Pan, Z. W.; Dai, Z. R.; Wang, Z. L. Nanobelts of semiconducting oxides. *Science* **2001**, *291*, 1947–1949.

[17] Kong, X. Y.; Ding, Y.; Yang, R.; Wang, Z. L. Single-crystal nanorings formed by epitaxial self-coiling of polar nanobelts. *Science* **2004**, *303*, 1348–1351.

[18] Gao, P. X.; Ding, Y.; Mai, W.; Hughes, W. L.; Lao, C.; Wang, Z. L. Conversion of zinc oxide nanobelts into superlattice-structured nanohelices. *Science* **2005**, *309*, 1700–1704.

[19] Wang, Z. L.; Kong, X. Y.; Zuo, J. M. Induced growth of asymmetric nanocantilever arrays on polar surfaces. *Phys. Rev. Lett.* **2003**, *91*, 185502.

[20] Pan, Z. W.; Mahurin, S. M.; Dai, S.; Lowndes, D. H. Nanowire array gratings with ZnO combs. *Nano Lett.* **2005**, *5*, 723–727.

[21] Gao, P. X.; Wang, Z. L. Nanopropeller arrays of zinc oxide. *Appl. Phys. Lett.* **2004**, *84*, 2883–2885.

[22] Tian, B.; Xie, P.; Kempa, T. J.; Bell, D. C.; Lieber, C. M. Single-crystalline kinked semiconductor nanowire superstructures. *Nat. Nanotechnol.* **2009**, *4*, 824–829.

[23] Pacholski, C.; Kornowski, A.; Weller, H. Self-assembly of ZnO: From nanodots to nanorods. *Angew. Chem. Int. Edit.* **2002**, *41*, 1188–1191.

[24] Kresse, G.; Hafner, J. *Ab initio* molecular dynamics for open-shell transition metals. *Phys. Rev. B* **1993**, *48*, 13115–13118.

[25] Kresse, G.; Furthmüller, J. Efficiency of *ab-initio* total energy calculations for metals and semiconductors using a plane-wave basis set. *Comp. Mater. Sci.* **1996**, *6*, 15–50.

[26] Wang, Y.; Perdew, J. P. Correlation hole of the spin-polarized electron gas, with exact small-wave-vector and high-density scaling. *Phys. Rev. B* **1991**, *44*, 13298–13307.

[27] Monkhorst, H. J.; Pack, J. D. Special points for Brillouin-zone integrations. *Phys. Rev. B* **1976**, *13*, 5188–5192.

[28] Geng, B. Y.; Wang, G. Z.; Jiang, Z.; Xie, T.; Sun, S. H.; Meng, G. W.; Zhang, L. D. Synthesis and optical properties of S-doped ZnO nanowires. *Appl. Phys. Lett.* **2003**, *82*, 4791–4793.